Co-published by
Institute of Fluid-Flow Machinery
Polish Academy of Sciences
Committee on Thermodynamics and Combustion
Polish Academy of Sciences

http://www.imp.gda.pl/archives-of-thermodynamics/

Thermophysical properties and microstructure of 32CrMoV12-28 hot-work tool steel

Piotr Koniorczyk[a], Mateusz Zieliński[a], Judyta Sienkiewicz[a*], Janusz Zmywaczyk[a]

[a]Military University of Technology, Faculty of Mechatronics, Armament and Aerospace, gen. Sylwestra Kaliskiego 2, 00-908 Warsaw, Poland
*Corresponding author email: judyta.sienkiewicz@wat.edu.pl

Received: 09.01.2024; revised: 21.02.2024; accepted: 03.03.2024

Abstract

Measurements of thermal diffusivity, heat capacity and thermal expansion of hot work tool steel 32CrMoV12-28 have been carried out in the temperature range from room temperature (RT) to 1000°C. 32CrMoV12-28 steel has been tested for military applications as steel for gun barrels. The thermophysical properties of this steel can be used as input data for numerical simulations of heat transfer in gun barrels. Both the LFA 427 laser flash apparatus in the RT–1000°C temperature range and the LFA 467 light flash apparatus in the RT–500°C temperature range were used for thermal diffusivity tests. Specific heat capacity was investigated in the range RT–1000°C. The specific heat was determined by two methods, i.e. the classical method, the so-called continuous-scanning method and the stepwise-scanning method according to EN ISO 11357-4. The paper compares both methods and assesses their suitability for testing the specific heat capacity of barrel steels. Thermal expansion was investigated in the range RT–1000°C. Inconel 600 was selected as the reference material during the thermal diffusivity test using LFA 467. Light microscopy (LM), scanning electron microscopy (SEM), and Vickers microhardness measurements were performed to detect changes in the microstructure before and after thermophysical measurements. We compared the results of measurements of the thermophysical properties of 32CrMoV12-28 steel with the results of our tests for other barrel steels with medium carbon content, i.e. X37CrMoV5-1 (1.2343), 38HMJ (1.8509) and 30HN2MFA. The comparison was made in terms of shifting the effect of material shrinkage towards higher temperatures.

Keywords: Microstructure; Thermal expansion; Thermal diffusivity; Specific heat capacity; 32CrMoV12-28 (1.2365) steel

Vol. 45(2024), No. 2, 269–277; doi: 10.24425/ather.2024.150871

Cite this manuscript as: Koniorczyk, P., Zieliński, M., Sienkiewicz, J., & Zmywaczyk, J. (2024). Thermophysical properties and microstructure of 32CrMoV12-28 hot-work tool steel. *Archives of Thermodynamics*, 45(2), 269–277.

1. Introduction

The durability of anti-aircraft guns in which gas flows at high pressure (of the order of hundreds of MPa) and high temperature (of the order of thousands of Kelvin) is influenced by mechanical erosion and changes in the thermophysical properties of steel. This damage manifests as a network of cracks as well as degradation of the Cr protective coating [1–5]. Thermal loads occurring during the operation of the barrel influence the microstructure, e.g. related to the ferrite-austenite phase transition of the barrel steel leading to a change in its mechanical properties [6–9]. The abovementioned phase transition during the heating and cooling of steel is associated with a sharp change in volume that in turn is caused by a transition from the BCC (body-

Nomenclature

A – thermal diffusivity, mm^2/s
c_p – specific heat, J/(kg K)
CLTE – coefficient of linear thermal expansion, 1/K
CR – cooling rate, K/min
d – diameter, mm
HR – heating rate, K/min
k – thermal conductivity, W/(m K)
L – length, mm
M – mass, mg
Q – pulse energy
t – time, s
T – temperature, K
T_∞ – corrected detector signal
V – gain of the detector signal amplitude

Greek symbols
α – ferrite
γ – austenite
ε – relative elongation (thermal expansion
ρ – density, g/cm^3

Subscripts and Superscripts
ref – reference material
s – sample
0 – initial
st – sapphire
bl – base line

Abbreviations and Acronyms
BCC – body-centred cubic
DSC – differential scanning calorimetry
EDS – energy dispersive spectroscopy
FCC – face-centred cubic
HV – Vickers hardness
LM – light microscopy
RT – room temperature
SEM – scanning electron microscopy

centred cubic) crystallographic lattice to the FCC (face-centred cubic) [6,7,9]. Additionally, during the operation of a barrel when pressure increases, denser phases are favoured and hence the FCC structure (γ-austenite) is more stable than the BCC structure (α-ferrite). In summary, the combined action of heat and pressure causes the formation and spread of deep cracks through the barrel and consequently leads to the destruction of the chrome coating on the inner surface of the barrel steel.

The authors' previous research on the coefficient of linear thermal expansion (CLTE) of similar barrel steels with medium carbon content, i.e. 30HN2MFA, 38HMJ (1.8509) and X37CrMoV5-1 (1.2343) showed that the ferrite-austenite phase transition and shrinkage effect occur at temperatures of 749.7 C, 808.4°C and 860.9°C [8,10,11]. Steels with a higher phase transformation temperature seem promising, i.e. X37CrMoV5-1 steel is better than 30HN2MFA steel. Heating such barrel steels to a temperature of 900°C and then slowly cooling causes irreversible changes in the ferrite and pearlite structure together with the characteristic Widmanstätten phases, resulting in reduced impact strength compared to the original steel [12,13]. Modern cannons fire according to a precisely defined sequence of shots, which is closely related to the shrinkage temperature of the cannon barrel steel. Therefore, designers of cannons and small arms look for steels in which this effect does not occur, or the shrinkage temperature of the barrel steel is as high as possible [10,14–20].

Another problem is the proper preparation of input data for the numerical simulation of heat transfer in the cannon barrel, especially thermal characteristics such as thermal conductivity k, specific heat c_p, density ρ and thermal diffusivity a. These parameters are related to each other through $a = k/(\rho c_p)$, and each can be measured separately or calculated from other parameters. When calculating the thermal conductivity k in the phase transition region, this effect is taken into account twice in both thermal diffusivity and specific heat. The authors of this paper suggest that the phase transition effect should only be included in the thermal conductivity characteristics [10,21].

The work aimed to investigate the thermophysical properties of the 32CrMoV12-28 (1.2365) hot work tool steel with the medium carbon content, in which, apart from the phase transition at the Curie point, there is a ferrite-austenite phase transition and the associated material shrinkage occurrence. To identify this transition, the DSC (differential scanning calorimetry) stepwise scanning method according to EN ISO 11357-4 was used, which allowed it to qualify as a first-order phase transition. According to the Ehrenfest nomenclature, the phase transition of the first kind is accompanied by the heat of the phase transition [6]. In addition to the specific heat, other thermophysical properties of this steel were also tested, i.e. thermal diffusivity and thermal expansion in the temperature range from RT (room temperature) to 1000°C. The thermophysical properties of the hot working 32CrMoV12-28 tool steel will be used as input data for the numerical simulation of heat transfer in a 35 mm cannon barrel, analogous to those of steels with medium carbon content, i.e. 30HN2MFA, 38HMJ (1.8509) and X37CrMoV5-1 (1.2343) [22–27]. As part of the paper, the authors also compared 32CrMoV12-5 steel with previously tested barrel steels with medium carbon content, looking for the relationship between the shrinkage temperature and the chromium content in these steels. This paper is a summary of research on the thermophysical properties of barrel steels with medium carbon content conducted by the authors from 2020 to the present [8,10,18,28].

2. Materials and methods

2.1. Materials

The 32CrMoV12-28 hot-work tool steel bar (Akrostal, Rogozno, Poland) supplied for testing was cylindrical with a length of 500 mm and a diameter of 71 mm. The tests were performed without additional heat treatment. The nominal composition (wt. %) of the test steel (32CrMoV12-28) is given in Table 1.

Table 1. Chemical composition of the hot-work tool (32CrMoV12-28) steel [7].

Component	Fe	C	Si	Mn
Concentration [wt. %]	92.88	0.32	0.25	0.30
Component	Cr	Mo	V	P
Concentration [wt. %]	3.00	2.75	0.55	0.03

32CrMoV12-28 is a high-alloy steel primarily used for making hot work tools, such as cutting and punching tools, dies and knives [29]. Generally, 32CrMoV12-28 is a high-performance tool steel engineered for applications where good toughness, wear resistance and high hardness are required, especially at lower temperatures. It can be heat-treated to achieve the desired mechanical properties for various tooling and cutting applications [7, 29]. As shown by the research described in this paper, compared to 38HMJ and 30HN2MFA steel, 32CrMoV12-28 steel is characterized by a higher ferrite-austenite transformation temperature, which is approximately 835.8°C. Only for X37CrMoV5-1 steel, shrinkage occurs at a higher temperature, i.e. 860.9°C.

2.2. Sample preparation

For the thermal diffusivity tests, cylindrical specimens with a thickness of 1.63 mm and a diameter of 12.70 mm were cut from a rod with a diameter of 71 mm. To increase the absorption of the energy of the heat pulse generated by the xenon lamp or laser, the samples were coated with a thin layer of graphite 2–3 µm thick (Graphit 33 Kontakt Chemie). The density of the materials was determined on a Sartorius MSA125P-1CE-DA analytical balance (accuracy [d]: 0.01 mg) using the double weighing method (in air and water). The result of measuring the density of the hot work tool steel at room temperature was 7.80 g/cm^3.

Cylindrical samples with a diameter of d = 6 mm and a mass of m = 191.3 mg for the test material and m = 114 mg for the reference material were used for DSC investigations. During the measurement, both samples were placed in a platinum crucible with a platinum lid (Pt crucible volume: 85 µl).

The samples for the dilatometric test had also cylindrical shapes with a diameter of 6.0 mm and length of 24.35 mm for hot-work tool steel (32CrMoV12-28). All samples were cut from the bar using a water-cooled cutting disc.

2.3. Microstructure analysis and Vickers micro-hardness measurements

The preparation of metallographic samples involved several steps. Initially, samples were cut using a precision cut-off machine and subsequently embedded in thermosetting Bakelite resin. Next, a sequence of abrasive treatments was applied, including grinding with 320-grit SiC paper and polishing using diamond pastes with particle sizes of 6, 3, and 1 µm. A final polishing step utilized 0.25 µm silica. The resulting microstructures were examined using two microscopy methods. The Keyence VHX-6000 digital (light) microscope was employed for initial analysis. Additionally, the Phenom Pro-X scanning electron microscope (Thermo Fisher Scientific) was used. SEM was equipped with an energy dispersive spectroscopy (EDS) chemical composition analyzer and operated at an acceleration voltage of 15 kV. To enhance the visibility of specific features, samples underwent etching with nital.

To validate the mechanical properties of the 32CrMoV12-28 steel, Vickers micro-hardness measurements at ambient temperature were conducted. This involved applying a load of 1000 g with a loading time of 10 s for each indentation. The measurements were performed using the Qness Q10 A+ Micro Hardness Tester from ATM Qness GmbH, which is a part of Verder Scientific, located in Maastricht, the Netherlands. The mean value for hardness was calculated based on a minimum of ten measurements for each sample.

2.4. Thermal analysis

2.4.1. Thermal diffusivity measurement

Thermal diffusivity measurements were performed using devices from Netzsch (Selb, Germany). To compare the results, tests were carried out on two devices: LFA 427 (laser flash apparatus) and LFA 467 HyperFlash (light flash apparatus). Thermal diffusivity testing using LFA devices refers to the Parker method and involves generating a heat impulse by a laser (LFA 427) or a xenon lamp (LFA 467) on one side of a plane-parallel sample and measuring the temperature change on the other side of the sample. Thermal diffusivity is calculated using the standard Cape-Lehman model with pulse correction for which a theoretical curve is fitted to the measurement points obtained on the IR (infrared) detector (CdHgTe) [30]. The standard model includes the effects of heat loss through surface radiation in the context of the temperature change of the analysed sample. Thermal diffusivity measurements were carried out independently on two instruments: LFA 467 at RT–500°C and LFA 427 at RT–1000°C. For each temperature step, two measurements were made in an atmosphere of argon as an inert gas at a flow rate of 50 ml/min. Unlike LFA 427, LFA 467 enables specific heat and thermal conductivity of the material under test to be measured, because the design of LFA 467 allows measurements to be made for several samples simultaneously. To determine the specific heat using the comparative method, Inconel 600 was used as a reference material [31]. In the comparative method, we use the following Eq. (1) to determine the specific heat:

$$c_p^s(T) = \frac{T_\infty^{ref}}{T_\infty^s}\frac{\rho^{ref}}{\rho^s}\frac{d^{ref}}{d^s}\frac{Q^s}{Q^{ref}}\frac{V^s}{V^{ref}}\frac{d^{2,s}_{\text{orifice}}}{d^{2,ref}_{\text{orifice}}}c_p^{ref}(T), \quad (1)$$

where there are such parameters as corrected detector signal (T_∞), density of sample material (ρ), sample diameter (d), pulse energy (Q), gain of the detector signal amplitude (V), diameter of IR detector measurement field (d with orifice index) and specific heat at constant pressure (c_p); superscripts: ref – reference material, s – sample. The T_∞ parameter is proportional to the adiabatic temperature and takes into account surface heat losses. In the context of Eq. (1) and the thermal diffusivity value of the

test sample $a(T)$ obtained from LFA 467, the thermal conductivity $k^s(T)$ was determined using Eq. (2):

$$k^s(T) = \frac{\rho_0}{[1+\varepsilon(T)]^3}\, a(T)\, c_p^s(T), \tag{2}$$

where $\varepsilon(T)$ stands for the relative elongation of the sample (thermal expansion).

2.4.2. Dilatometric measurements

A Netzsch pusher dilatometer (DIL402C) was used to measure the thermal expansion of 32CrMoV12-28 steel. The experiment was conducted in the range from room temperature (RT) to 1100°C. As a protective gas, nitrogen was supplied to the measurement chamber at a gas flow rate of 60 ml/min. The thermal expansion of the sample, expressed by the coefficient of linear thermal expansion (CLTE), is practically represented regarding the initial sample length $L(T_0)$ – denoted as CLTE* and represented by Eq. (3) [31,32]:

$$\mathrm{CLTE}^*(T) = \frac{1}{L(T_0)}\frac{\mathrm{d}L(T)}{\mathrm{d}T} = \frac{1}{L_0}\frac{\mathrm{d}L(T)}{\mathrm{d}T}. \tag{3}$$

The heating rate (HR) was 2 K/min. The relative elongation mentioned in Eq. (2) is related to CLTE* as follows:

$$\mathrm{CLTE}^*(T) = \frac{1}{\mathrm{d}T}\frac{\mathrm{d}L(T)}{L_0} = \frac{1}{\mathrm{d}T}\mathrm{d}\varepsilon. \tag{4}$$

2.4.3. Differential scanning calorimeter measurement

The specific heat capacity temperature characteristics were determined using a DSC 404 F1 Pegasus differential scanning calorimeter (Netzsch). Two methods were used, i.e. the classic method of the continuous-scanning - in the range of RT to about 1000°C and the stepwise-scanning method according to EN ISO 11357-4 – in the range of 490°C to about 910°C [33]. In the classical DSC approach, the temperature characteristics of the heat capacity of the test material were determined using the c_p-ratio method from three DSC curves (test sample line, sapphire line, baseline) [31]. The test was carried out at a heating/cooling rate (HR/CR) of 10 K/min. In the case of the stepwise DSC method, the temperature rise was achieved through a sequence of isothermal and dynamic segments. The dynamic segments heated up at a rate of 10 K/min, and the isothermal segments lasted 10 min. The temperature increase during the dynamic section was 20°C. An initial dynamic segment was used to reach a first isothermal temperature of 490°C. The next isothermal segments were: 510°C, 550°C, 590°C, 650°C, 690°C, 710°C, 730°C, 750°C, 770°C, 790°C, 810°C, 830°C, 850°C, 870°C, 890°C. To avoid damage to the crucible/DSC sensor system, the maximum isothermal temperature segment was limited to 910°C. Similarly, to the classic DSC method, in the stepwise DSC method, 3-DSC curves (baseline, sapphire line and line of the tested sample) were used to determine the specific heat. The specific heat of the sample was calculated from the peak integrals of the DSC signals during dynamic temperature steps according to Eq. (5) [33]:

$$c_p^s = c_p^{st}\frac{m_{st}}{m_s}\frac{\Delta Q_s - \Delta Q_{bl}}{\Delta Q_{st} - \Delta Q_{bl}}, \tag{5}$$

where c_p^s is the specific heat capacity of the sample; c_p^{st} is the specific heat capacity of the sapphire; *s*, *st* and *bl* indices denote the sample, sapphire and baseline; ΔQ_s, ΔQ_{bl}, ΔQ_{st} are the integrals of the peak-shaped DSC signals during a dynamic temperature step; m_{st} and m_s are the masses of the sapphire and the sample.

Both in the classic method and in the stepwise method, the tests were carried out in a protective atmosphere of argon at a flow of 20 ml/min. To obtain stable DSC signals, two evacuations of argon filling the furnace chamber were used along with 15-minute isothermal segments at the beginning of the measurement.

3. Thermal analysis

3.1. Microstructural analysis

The typical microstructure of 32CrMoV12-28 hot-work steel is dependent on the performed heat treatment, i.e. quenching and tempering temperatures and times. The final microstructure and hence properties can be tailored to meet the desired mechanical and thermal requirements for a particular application.

The examined microstructure of as-received 32CrMoV12-28 steel is composed of tempered martensite, as a matrix, and precipitations of carbides (Fig. 1). Generally, tempered martensite is obtained when quenched steel is subjected to a tempering process to reduce the brittleness and improve toughness. This process involves reheating the steel to a specific temperature range and holding it for a certain period to transform some of the martensite into tempered martensite, which is less brittle and has improved ductility compared to the as-quenched martensite. Observed carbides are compounds of carbon with various alloying elements, i.e. chromium, vanadium, molybdenum and silicon, see Fig. 1 (EDS – element distribution map).

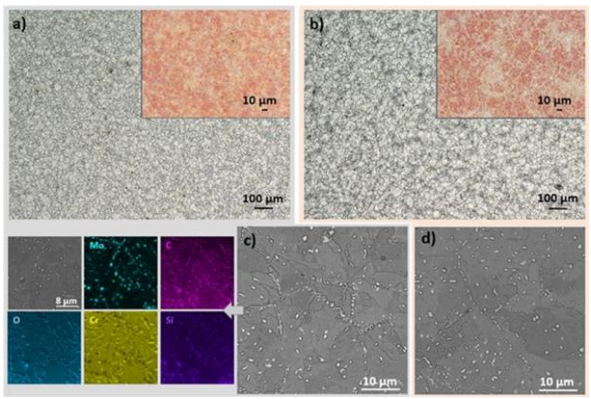

Fig. 1. Microstructure of 32CrMoV12-28 steel in a) initial state, b) after DCS measurement obtained by using a light microscope and c) initial state (together with an elements distribution map), d) after DCS measurement obtained by using SEM.

These carbides occur along grain boundaries as well as are dispersed throughout the tempered martensitic matrix. In both cases, they are elliptical or even spherical.

A slight reduction in hardness was observed after the DSC test. The hardness of the sample HV1 in the initial state was 194 ± 4, while it decreased to 190 ± 3 for the sample after the DSC measurement. This reduction may be due to an increase in the amount of martensite in the sample material after the DSC measurement.

3.2. Thermal properties investigations

The thermal expansion, specific heat capacity and thermal diffusivity of 32CrMoV12-28 steel were investigated from room temperature (RT) to about 1000°C. Measurements of the thermal diffusivity of the tested steel allowed for the identification of the Curie point temperature and changes in thermal diffusivity as a function of temperature. Only one measurement cycle was performed, as in the case of thermal expansion and specific heat using the classic continuous-scanning DSC method. In the case of stepwise scanning DSC method of the specific heat measurements (in the range 490–910°C), the tests were repeated twice to verify the measurement results.

Thermal diffusivity tests were carried out in stages. In the first stage, measurements were made from room temperature to 1000°C using an LFA 427 apparatus. The results of the thermal diffusivity measurements were obtained while the sample was being heated. In the second stage, thermal diffusivity measurements were also taken from room temperature to 480°C. For this purpose, the LFA 467 apparatus was used and the thermal diffusivity characteristics were determined during the heating of the samples. At the same time, for the steel sample, the thermal diffusivity of the reference material (Inconel 600) was also measured using LFA 467. This measurement was necessary to calculate the specific heat as a function of the temperature of the steel under test, using Eq. (1).

The DIL402C high-temperature dilatometer was used to measure thermal expansion. The measurements aimed to determine the thermal expansion characteristics of the test material from room temperature to 1000 °C during continuous heating at 2 K/min.

In the case of specific heat investigations, two methods were used, i.e. the classic continuous-scanning DSC method and the stepwise-scanning DSC method according to EN ISO 11357-4. In addition, a comparative method of measuring thermal diffusivity LFA 467 in the temperature range RT–500°C was used together with the apparent specific heat measurements DSC in the temperature range RT–1000°C, for specific heat calculations.

Netzsch Geräte GmbH guarantees the proper accuracy of its devices. This allows the determination of thermophysical properties of the tested material based on two to three measurements. To ensure sufficient accuracy, measurements on a reference material supplied by Netzsch with thermophysical characteristic tables must be performed before each measurement series. To verify the accuracy of the device, the thermophysical measurement results for the reference material are compared with the data from the tables. For thermal diffusivity measurements, the reference material was Inconel 600 and the deviation of the results did not exceed 5%. Sapphire was used in thermal expansion measurements. The deviation of the measurement results from Netzsch data did not exceed 4%. The same material was used in specific heat measurements. The accuracy did not exceed a 6% difference between the data provided by Netzsch and the data obtained from the reference sample measurements. Additionally, the device undergoes temperature calibration with the melting of pure elements (tin, zinc, silver, etc.) to improve measurement accuracy.

3.2.1. Thermal diffusivity investigations

The temperature characteristics of the thermal diffusivity of 32CrMoV12-28 steel obtained with both diffusometers (LFA427 and LFA467) are shown in Fig. 2. From the thermal diffusivity characteristics, it can be seen that at a temperature of about 764.8°C, there is a phase transition from the ferromagnetic to the paramagnetic state – the Curie point. As can be seen in Fig. 2, the thermal diffusivity of 32CrMoV12-28 decreases steadily with temperature up to the Curie point and reaches a minimum value of about 3 mm^2/s. Beyond the Curie point temperature, the thermal diffusivity increases with temperature.

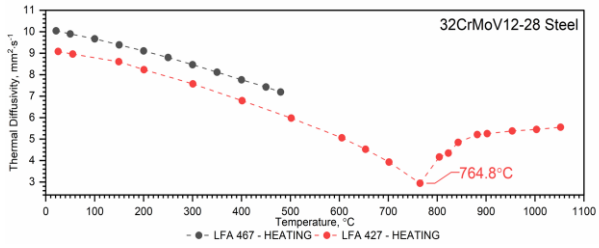

Fig. 2. Thermal diffusivity as a function of temperature for the 32CrMoV12-28 hot-work tool steel obtained from the first heating runs on LFA 467 and LFA 427 (based on [34]).

Figure 3 shows the dependence of thermal conductivity as a function of temperature, obtained by the comparative method in the RT–500°C range and using Eq. (2) in the RT–1000°C range. The differences between the two characteristics for the RT–500°C range are due to the lower accuracy of the thermal diffusivity determination (Fig. 2, black dashed line) using the LFA 467 apparatus.

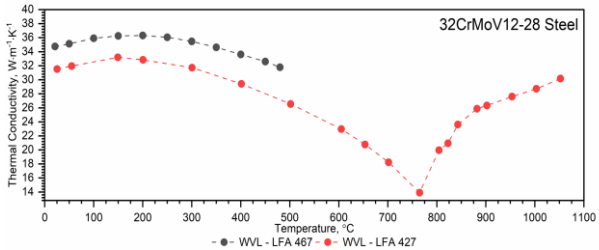

Fig. 3. Thermal conductivity as a function of temperature for the 32CrMoV12-28 hot-work tool steel obtained from the first heating runs on LFA 467 (black dotted line) and LFA 427 (red dotted line).

Figure 4 shows the dependence of specific heat as a function of temperature, obtained by a comparative method using LFA 467 from room temperature to 500°C, and obtained by approximation of experimental data from DSC in the RT–1000°C range.

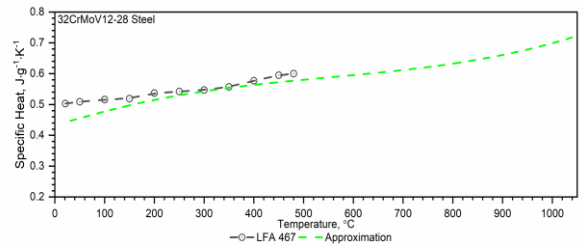

Fig. 4. Specific heat as a function of temperature for the 32CrMoV12-28 hot-work tool steel obtained from the first heating run on LFA 467 in the range from RT to about 500°C (dotted black line) and from the approximation of the experimental data on DSC in the range from RT to 1000°C (green dashed line).

3.2.2. Thermal expansion investigations

The DIL402C high-temperature dilatometer was used to measure the thermal expansion of the test steel from room temperature (RT) to 1000°C during continuous heating at a rate of 2 K/min. One measurement cycle was carried out for the sample. The temperature-dependent thermal expansion characteristics of 32CrMoV12-28 steel are shown in Fig. 5.

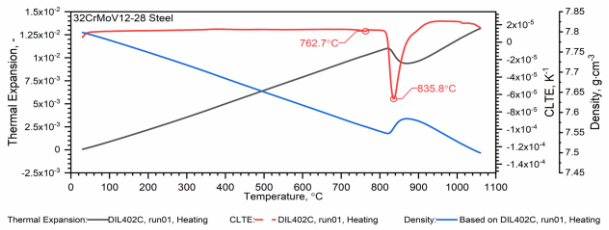

Fig. 5. Density, thermal expansion and CLTE as a function of temperature for the 32CrMoV12-28 hot-work tool steel obtained from the first heating run on DIL 402 C.

3.2.3. Differential scanning calorimeter investigations

The result of the classic continuous-scanning DSC method of the apparent specific heat investigations (calculated using the c_p-ratio method) based on the 3-DSC curves (baseline, sapphire line and tested sample line) for the 32CrMoV12-28 hot-work tool steel samples is shown in Fig. 6. One measuring cycle was carried out for the sample. The figure also shows the specific heat determined by the comparison method during thermal diffusivity measurements (LFA 467) in the RT–500°C range – dashed green line. The resulting specific heat was compared with the results of apparent specific heat measurements in the RT–1000°C range (DSC 404 F1 Pegasus – classic continuous-scanning method). The purple dashed line (Fig. 6) shows the specific heat as a function of temperature, described by Eq. (6). The thermal conductivity shown in Fig. 3 was calculated using Eq. (2) for which the specific heat values were determined from Eq. (6).

For 32CrMoV12-28 steel, a correlation formula was proposed for the specific heat capacity over the tested temperature range (RT–1000°C). The fitting curve for specific heat capacity as a function of temperature for the tested steel is shown in Fig. 6 as a dashed purple line, for which the proposed formula has the following form:

$$c_p(T) = a_0 + a_1 T + a_2 T^2 + a_3 T^3 + a_4 T^{\frac{1}{3}}, \qquad (6)$$

where the temperature is given in kelvins. The values of the coefficients are given in Table 2.

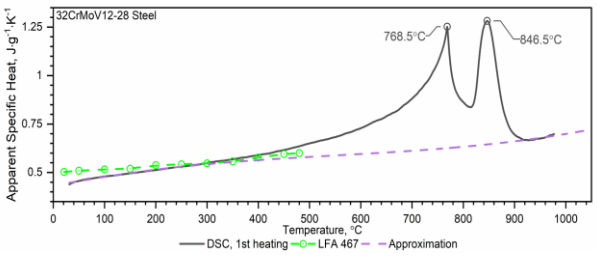

Fig. 6. Temperature characteristics of apparent specific heat for the 32CrMoV12-28 hot-work tool steel obtained from the first heating run: dotted green line—results obtained from LFA 467; dashed purple line—approximation of measurement from DSC; black line – results obtained from classic continuous-scanning DSC method.

Table 2. Coefficients for calculating specific heat capacity of 32CrMoV12-28 sample on Eq. (5).

Coefficient	Value	Coefficient	Value
a_0[J/(g K)]	4.1470×10^{-1}	a_3[J/(g K^4)]	4.8932×10^{-2}
a_1[J/(g K^2)]	6.0408×10^{-4}	a_4[J/(g K$^{2/3}$)]	4.5697×10^{-2}
a_2[J/(g K^3)]	-8.1376×10^{-7}		

To sum up, the input data for numerical simulations of heat transfer in the barrel related to the thermophysical properties of steel will be used: specific heat in the form of a polynomial Eq. (6), the dependence of thermal conductivity as a function of temperature presented in the form of a red dotted line in Fig. 3, and the dependence of density as a function of temperature illustrated in the form of a blue line in Fig. 5.

A comparison of the results of the stepwise-scanning DSC method with the results of the classic continuous-scanning DSC method for the same steel is shown in Fig. 7. Two measuring

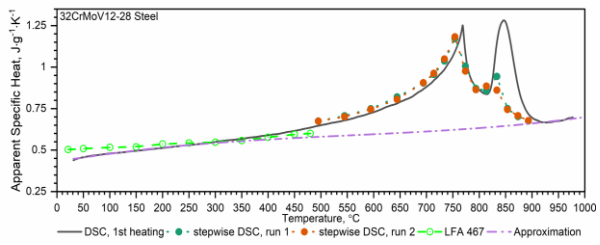

Fig. 7. Temperature characteristics of apparent specific heat for 32CrMoV12-28 obtained from: the first heating run by the classic continuous scanning DSC method – black line; the first and second heating runs by the stepwise-scanning DSC method – blue and red points together with the characteristic of specific heat obtained from LFA 467 – dashed green line.

cycles were carried out for the sample in the temperature range 490÷900°C in the case of the stepwise scanning DSC method.

Repeated thermostating of the sample in the stepwise-scanning DSC method removes the peak associated with the shrinkage temperature of the tested steel, i.e. 846.5°C, because this type of phase transformation requires the supply of heat. The first peak, i.e. 768.5°C, remains practically in the same place as in the classic continuous-scanning DSC method, because it is related to the phase transition at the Curie temperature.

Both methods of measuring apparent specific heat, i.e. the classic method, the so-called continuous-scanning DSC method and the stepwise DSC method – under the EN ISO 11357-4 standard, are complementary. Thermostating the sample also allows for a better understanding of the results of measurements of thermal diffusivity of barrel steels as a function of temperature.

3.2.4. Comparison of thermophysical properties of selected barrel steels

Figure 8 presents a summary of the results of measurements of thermophysical properties, i.e. thermal diffusivity, thermal expansion and apparent specific heat as a function of temperature for selected barrel steels with medium carbon content, i.e. 30HN2MFA, 38HMJ, X37CrMoV5-1, 32CrMoV12-28. All these measurements were performed using various methods [8–10]. Measurements of thermal diffusivity using the laser flash method (LFA 427) required thermostating the sample to the measurement temperature, which made it impossible to record changes in this parameter during the phase transition associated with the shrinkage effect of the steel. However, thermosetting the sample at the measurement temperature did not affect the registration of the thermal diffusivity of phase transitions at the Curie temperature. In the case of measurements of apparent specific heat using the continuous scanning DSC method and thermal expansion using the pushrod dilatometer method, peaks related to steel shrinkage were also recorded (Fig. 8). Thermostating of the sample did not prevent the recording of changes in thermal diffusivity as a function of temperature during the second type of phase transition, i.e. the transition of steel from the ferromagnetic state to the paramagnetic state at the Curie point, because the heat of this phase transition is zero. The identification of the phase transition at the Curie point as a phase transition of the second type was also confirmed by measurements of the apparent specific heat using the stepwise DSC method, which also required thermostating of the sample at the measurement temperature (Fig. 7).

In the case of 30HN2MFA steel, both transformations, i.e. Curie and shrinkage, coincide, which is confirmed by the measurements of thermal expansion of this steel (Fig. 8). It is also worth noting that despite the different heating rates of the sample using the DSC method, i.e. 10 K/min, and thermal expansion, i.e. 2 K/min, the shrinkage temperatures obtained by both methods practically coincide. Differences in the determination of shrinkage effect temperature reach approximately 3°C.

Figure 9 shows the steel shrinkage temperature as a function of the chromium content for selected barrel steels with medium carbon content, i.e. 30HN2MFA, 38HMJ, X37CrMoV5-1, 32CrMoV12-28. It is also worth noting that the higher the Cr content in the steel, the higher the shrinkage temperature (Fig. 8 and Table 3).

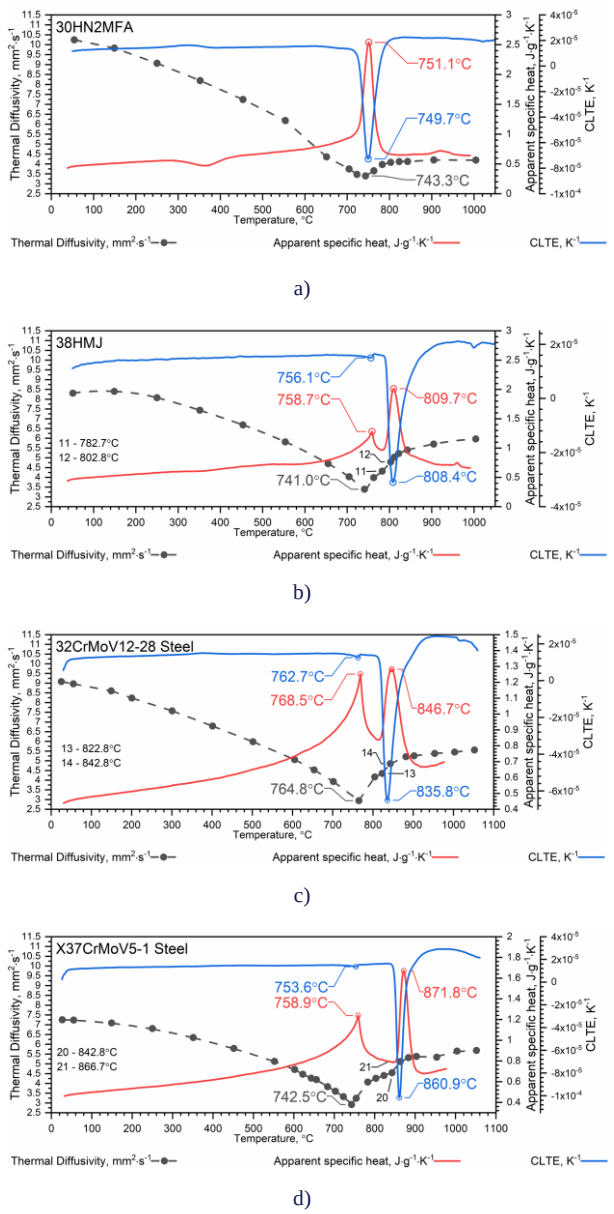

Fig. 8. Thermal diffusivity, CLTE and apparent specific heat of selected barrel steels (based on [8,10]).

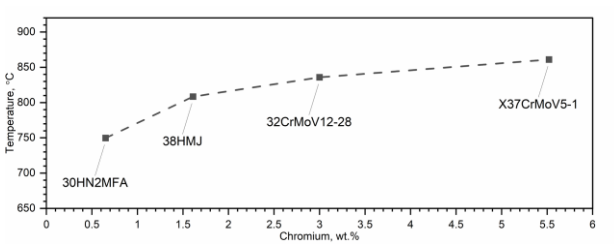

Fig. 9. Influence of chromium content on shrinkage temperature of selected barrel steels, i.e. 30HN2MFA, 38HMJ, 32CrMoV12-28, X37CrMoV5-1 [8,10,35,36].

Table 3. Chemical composition of tested steels [8,10].

Steel grade	Chemical composition [wt. %]				
	Fe	C	Si	Mn	Cr
30HN2MFA	96.42	0.29	0.26	0.36	0.65
38HMJ	95.21	0.44	0.24	0.54	1.61
32CrMoV12-28	92.88	0.32	0.25	0.30	3.00
X37CrMoV5-1	90.71	0.39	0.84	0.36	5.52
	Mo	Ni	V	Al	P
30HN2MFA	0.24	2.21	0.23	—	—
38HMJ	0.26	0.19	1.20	1.20	—
32CrMoV12-28	2.75	—	0.55	—	0.03
X37CrMoV5-1	1.30	0.40	0.45	—	0.012

4. Conclusions

The authors analyzed the thermophysical properties of medium-carbon barrel steel 32CrMoV12-28 and compared it with other previously measured barrel steels, i.e. 30HN2MFA, 38HMJ, X37CrMoV5-1, manufactured on behalf of arms factories. In all of them, apart from the phase transition associated with the Curie point, the ferrite-austenite phase transition occurs. This phenomenon is related to material shrinkage (the transformation into austenite) and occurs in the tested steels at various temperatures. It is widely known that chromium influences the shrinkage temperature in medium carbon hot-work steels which in turn refers to the phase transformation behavior of such steels. The transformation of ferrite into austenite is determined by several alloying elements, including chromium, and can affect the shrinkage temperature, which is the temperature at which this transformation occurs during cooling or heating. Chromium is a ferrite stabilizer which means, that it tends to promote the formation of ferrite in steel. Hence, it can increase the temperature at which austenite transforms into ferrite during cooling. It implies that the addition of chromium can lead to a higher shrinkage temperature, as the transformation from austenite to ferrite will occur at a higher temperature. Furthermore, chromium also has a strong affinity for carbon, and hence it forms carbides that can act as nucleation sites for phase transformations, affecting the kinetics of the transformation. Express differently, the presence of chromium carbides can potentially raise the shrinkage temperature. It should be borne in mind, however, that the exact influence of chromium on the shrinkage temperature in medium carbon hot-work steels can vary depending on the specific composition of the steel, including the presence of other alloying elements such as nickel, manganese, molybdenum, vanadium, and chromium. Additionally, the heat treatment process, cooling rate, and other factors can also have an impact on the transformation behaviour and shrinkage temperature. Summarizing this part, chromium in medium carbon hot-work steels raises the shrinkage temperature by promoting the formation of ferrite and influencing the nucleation of phase transformations. Nevertheless, it is important to remember that the precise effect depends on the overall steel composition and processing conditions.

Another problem is the measurement of the specific heat of the tested steel. According to Ehrenfest's classification, the effect of material shrinkage is a phase transition of the first type, i.e. a transition associated with the heat of transformation. To identify this effect, the authors used the stepwise scanning method in DSC studies. Thermostating of the measurement sample near the material shrinkage temperature, which is associated with the supply of phase transition heat, practically eliminates the peak associated with the characteristics of the apparent specific heat obtained in the classic method of continuous scanning DSC measurement. It should be noted that the thermostating of the sample does not affect the peak related to the Curie point temperature, because the heat of this transformation is equal to zero.

As a result, it can be concluded that an analogous character of temperature-dependent changes in thermophysical properties is observed in steels with medium carbon content. The thermal diffusivity and thermal conductivity of these steels decrease monotonically with increasing temperature until the Curie point is reached, for which they reach a minimum value. The values of both parameters increase above the ferromagnetic-paramagnetic phase transition temperature. However, the increase in the values of these parameters is small. Two peaks are observed in the apparent specific heat results. The first endothermic peak is related to the Curie point temperature (ferromagnetic-paramagnetic transition). The second peak is related to the ferrite-austenite phase transition. For 30HN2MFA steel, we observe the overlap of the peaks of these two transitions (Curie point temperature and ferrite-austenite transition).

The analysis of the influence of steel shrinkage temperature as a function of chromium content allowed for ranking the selected barrel steels with medium carbon content, i.e. 30HN2MFA, 38HMJ, X37CrMoV5-1, 32CrMoV12-28 in terms of their suitability for military applications. The least useful steel is currently the most commonly used, i.e. 30HN2MFA, because the shrinkage temperature of this steel is the lowest and is 749.7°C. The best steel for barrels is X37CrMoV5-1 because the shrinkage temperature of this steel is approximately 860.9°C, which allows for more heat impulses (shots). The 32CrMoV12-28 steel analyzed in this work has a shrinkage temperature of 835.8°C, which makes it as attractive as the X37CrMoV5-1 steel.

References

[1] Sopok, S., Rickard, C., & Dunn, S. (2005). Thermal-chemical-mechanical gun bore erosion of an advanced artillery system part one: Theories and mechanisms. *Wear*, 258(5-6), 659–670. doi: 10.1016/j.wear.2004.09.031

[2] Sopok, S., Rickard, C., & Dunn, S. (2005). Thermal–chemical–mechanical gun bore erosion of an advanced artillery system part two: Modeling and predictions. *Wear*, 258(5-6), 671–683. doi: 10.1016/j.wear.2004.09.030

[3] Li, H., Chen, G., Zhang, K., Luo, G., & Ye, Z. (2007). Degradation failure features of chromium-plated gun barrels with a laser-discrete-quenched substrate. *Surface and Coatings Technology*, 201(16-17), 9558–9564. doi: 10.1016/j.surfcoat.2007.04.034

[4] Sarraf, S. H., Soltanieh, M., & Aghajani, H. (2016). Repairing the cracks network of hard chromium electroplated layers using plasma nitriding technique. *Vacuum*, 127, 1–9. doi: 10.1016/j.vacuum.2016.02.001

[5] Dębski, A., Surma, Z., & Koperski, W. (2009). Material and technological optimization research in terms of increasing the durability of small arms. *Journal of Physics: Conference Series*, 2628, 012035. doi: 10.1088/1742-6596/2628/1/012035

[6] Bhadeshia, H.K.D.H. (2021). *Theory of transformations in steels*. Boca Raton: CRC Press.

[7] Blicharski, M. (2017). *Inżynieria materiałowa: Stal* (2nd ed., 1st reprint). Warszawa: Wydawnictwo WNT. ISBN 9788301189556.

[8] Koniorczyk, P., Zmywaczyk, J., Dębski, A., Zieliński, M., Preiskorn, M., & Sienkiewicz, J. (2020). Investigation of thermophysical properties of three barrel steels. *Metals*, 10(5), 573. doi: 10.3390/met10050573

[9] Koniorczyk, P., Zmywaczyk, J., Dębski, A., Zieliński, M., & Cegła, M. (2019). Investigations of thermal diffusivity and thermal expansion for three types of barrel steel. *Thermophysics 2019: 24th International Meeting of Thermophysics and 20th Conference REFRA* (p. 20006). Smolenice, Slovakia, AIP Publishing.

[10] Koniorczyk, P., Zieliński, M., Sienkiewicz, J., Zmywaczyk, J., & Dębski, A. (2023). Experimental studies of thermophysical properties and microstructure of X37CrMoV5-1 hot-work tool steel and maraging 350 steel. *Materials*, 16(3), 1206. doi: 10.3390/ ma16031206

[11] Kaschnitz, E., Hofer-Hauser, P., & Funk, W. (2020). Electrical resistivity measured by millisecond pulse-heating in comparison to thermal conductivity of the hot work tool steel AISI H11 (1.2343) at elevated temperature. *High Temperatures-High Pressures: Thermophysical Properties: Fundamentals and Applications*, 49, 75–87. doi: 10.32908/hthp.v49.825

[12] Souza, S. d. S. d., Moreira, P.S., & Faria, G.L. d. (2020). Austenitizing temperature and cooling rate effects on the martensitic transformation in a microalloyed-steel. *Materials Research*, 23, 322. doi: 10.1590/1980-5373-MR-2019-0570

[13] Coll Ferrari, M.T. (n.d.). Effect of austenitising temperature and cooling rate on microstructures of hot-work tool steels. https://www.diva-portal.org/smash/get/diva2:868510/ FULLTEXT01.pdf [accessed 27 Oct. 2023].

[14] Tewari, R., Mazumder, S., Batra, I.S., Dey, G.K., & Banerjee, S. (2000). Precipitation in 18 wt% Ni maraging steel of grade 350. *Acta Materialia*, 48, 1187–1200. doi: 10.1016/S1359-6454(99)00370-5

[15] Guo, Z., Sha, W., & Li, D. (2004). Quantification of phase transformation kinetics of 18 wt.% Ni C250 maraging steel. *Materials Science and Engineering: A*, 373, 10–20. doi: 10.1016/ j.msea. 2004.01.040

[16] Jarfors, A.E.W., Matsushita, T., Siafakas, D., Stolt, R. (2021). On the nature of the anisotropy of Maraging steel (1.2709) in additive manufacturing through powder bed laser-based fusion processing. *Materials & Design*, 204, 109608. doi: 10.1016/ j.matdes. 2021.109608

[17] Kapoor, R., Kumar, L., & Batra, I.S. (2003). A dilatometric study of the continuous heating transformations in 18wt.% Ni maraging steel of grade 350. *Materials Science and Engineering: A*, 352, 318–324. doi: 10.1016/S0921-5093(02)00934-6

[18] Koniorczyk, P., Sienkiewicz, J., Zmywaczyk, J., Dębski, A., Zieliński, M., & Preiskorn, M. (2021). Effect of microstructure on thermophysical properties of heat-treated duplex steel. *Materials (Basel)*, 14(20), 6043. doi: 10.3390/ma14206043

[19] Knyazeva, M., & Pohl, M. (2013). Duplex Steels: Part I: Genesis, Formation, Structure. *Metallography, Microstructure, and Analysis*, 2, 113–121. doi: 10.1007/s13632-013-0066-8

[20] Knyazeva, M., & Pohl, M. (2013). Duplex Steels. Part II: Carbides and Nitrides. *Metallography, Microstructure, and Analysis*, 2, 343–351. doi: 10.1007/s13632-013-0088-2

[21] Chen, H., Yue, Z., Ren, D., Zeng, H., Wei, T., Zhao, K., Yang, R., Qiu, P., Chen, L., & Shi, X. (2019). Thermal conductivity during phase transitions. *Advanced Materials*, 31(51), e1806518. doi: 10.1002/adma.201806518

[22] Zieliński, M., Koniorczyk, P., Surma, Z., Zmywaczyk, J., & Preiskorn, M. (2022). Numerical study of heat transfer in a gun barrel made of selected steels. *Energies*, 15(5), 1868. doi: 10.3390/ en15051868

[23] Fikus, B., Dorochowicz, A., Surma, Z., Kijewski, J., Leciejewski, Z., Michalski, J., & Trębiński, R. (2022). Investigations of middle-caliber anti-aircraft cannon interior ballistics including heat transfer problem in estimation of critical burst length. *Processes*, 10(3), 607. doi: 10.3390/pr10030607

[24] Dębski, A., Koniorczyk, P., Leciejewski, Z., Preiskorn, M., Surma, Z., & Zmywaczyk, J. (2016). Analysis of heat transfer in a 35 mm barrel of an anti-aircraft cannon. *Problems of Mechatronics: Armament, Aviation, Safety Engineering*, 7, 71–86. doi: 10.5604/01.3001.0009.2983

[25] Fikus, B., Surma, Z., Leciejewski, Z., & Trębiński, R. (2022). Influence of relations defining propellant gases-barrel heat transfer on critical burst length of 35 mm anti-aircraft cannon. *Proceedings of the 32nd International Symposium on Ballistics*, May 9-13, 2022 (pp. 71–86). DEStech Publications.

[26] Zieliński, M., Koniorczyk, P., Surma, Z., Preiskorn, M., & Sienkiewicz, J. (2023). Selected aspects of heat transfer study in a gun barrel of an anti-aircraft cannon. *Problems of Mechatronics: Armament, Aviation, Safety Engineering*, 14, 73–86. doi: 10.5604/ 01.3001.0053.6672

[27] Koniorczyk, P., Zieliński, M., & Surma, Z. (2023). Heat transfer in the anti-aircraft gun barrel during fire with training and combat ammunition – Comparison of calculation results. *Issues of Armament Technology*, 165(3), 23–39. doi: 10.5604/01.3001. 0053.9191

[28] Zieliński, M., & Koniorczyk, P. (2023). Thermophysical properties of selected barrel steels. *Issues of Armament Technology*, 164(2), 19–41. doi: 10.5604/ 01.3001.0053.7229

[29] Mesquita, R. A. (2016). *Tool steels*. CRC Press. ISBN 9781439881729.

[30] Cape, J.A., & Lehman, G.W. (1963). Temperature and finite pulse-time effects in the flash method for measuring thermal diffusivity. *Journal of Applied Physics*, 34(7), 1909–1913. doi: 10.1063/1.1729711

[31] Netzsch. (2023). *Proteus ver. 7.1 software manual*. https://www.netzsch-thermal-analysis.com/en/products-solutions/software/proteus/ (accessed 27 Oct. 2023).

[32] Ling, S.J., Sanny, J., & Moebs, W. (2018). *University physics, vol. 2*. OpenStax, Rice University.

[33] Schindler, A. (2023). *"Stepwise" According to EN ISO 11357-4*. https://analyzing-testing.netzsch.com/_Resources/Persistent/3/0/4/8/3048e6366e9773455694482cc4f15f72da7d65bd/SW%20Innovation%20014_English.pdf [accessed 27 Oct. 2023].

[34] Zieliński, M., & Koniorczyk, P. (2023). Thermal diffusivity and thermal expansion investigations of WLV steel. *Journal of Physics: Conference Series*, 2628(1), 012035. doi: 10.1088/1742-6596/2628/1/012035

[35] Chadha, K., Shahriari, D., Aranas, C., Lapierre-Boire, L.-P., & Jahazi, M. (2019). On the role of chromium in dynamic transformation of austenite. *Metals and Materials International*, 25, 559–569. doi: 10.1007/s12540-018-00227-6

[36] Jirková, H., Kučerová, L., & Mašek, B. (2015). The effect of chromium on microstructure development during Q-P process. *Materials Today: Proceedings*, 2, 627–630. doi: 10.1016/ j.matpr. 2015.07.362